Biochimica et Biophysica Acta xxx (2012) xxx–xxx

Contents lists available at SciVerse ScienceDirect

Biochimica et Biophysica Acta

journal homepage: www.elsevier.com/locate/bbapap

Frataxin from *Psychromonas ingrahamii* as a model to study stability modulation within the CyaY protein family

Ernesto A. Roman [a], Santiago E. Faraj [a], Alexandra Cousido-Siah [b], André Mitschler [b], Alberto Podjarny [b], Javier Santos [a,*]

[a] Instituto de Química y Fisicoquímica Biológicas, Universidad de Buenos Aires, Junín 956, C1113AAD, Buenos Aires, Argentina
[b] Department of Integrative Biology, IGBMC, CNRS, INSERM, Université de Strasbourg, Illkirch, France

ARTICLE INFO

Article history:
Received 13 November 2012
Received in revised form 26 January 2013
Accepted 11 February 2013
Available online xxxx

Keywords:
Protein flexibility
Protein stability
Protein dynamics
Stability modulation
Crystallography
Molecular dynamics simulations

ABSTRACT

Adaptation of life to low temperatures influences both protein stability and flexibility. Thus, proteins from psychrophilic organisms are excellent models to study relations between these properties. Here we focused on frataxin from *Psychromonas ingrahamii* (pFXN), an extreme psychrophilic sea ice bacterium that can grow at temperatures as low as −12 °C. This α/β protein is highly conserved and plays a key role in iron homeostasis as an iron chaperone. In contrast to other frataxin homologs, chemical and temperature unfolding experiments showed that the thermodynamic stability of pFXN is strongly modulated by pHs: ranging from 5.5 ± 0.9 (pH 6.0) to 0.9 ± 0.3 kcal mol^{-1} (pH 8.0). This protein was crystallized and its X-ray structure solved at 1.45 Å. Comparison of B-factor profiles between *Escherichia coli* and *P. ingrahamii* frataxin variants (51% of identity) suggests that, although both proteins share the same structural features, their flexibility distribution is different. Molecular dynamics simulations showed that protonation of His44 or His67 in pFXN lowers the mobility of regions encompassing residues 20–30 and the C-terminal end, probably through favorable electrostatic interactions with residues Asp27, Glu42 and Glu99. Since the C-terminal end of the protein is critical for the stabilization of the frataxin fold, the predictions presented may be reporting on the microscopic origin of the decrease in global stability produced near neutral pH in the psychrophilic variant. We propose that suboptimal electrostatic interactions may have been an evolutionary strategy for the adaptation of frataxin flexibility and function to cold environments.

1. Introduction

Close inspection of the molecular biology of extremophilic organisms and their macromolecular components may give a clue about their adaptive strategies. In the case of psychrophilic microorganisms, these include *general solutions* like the production of anti-freeze [1,2] and cold-shock proteins [3], alterations in membrane composition, and overexpression of proteins that destabilize DNA structures [4], among other mechanisms. In addition, cellular adaptations occur, such as osmolyte synthesis (e.g., glycerol and trimethylamine N-oxide), incorporation of specific lipids, and macromolecular crowding [4,5]. However, proteins from extreme environments usually display differences in their stability and functional temperature. We refer to these kinds of solutions as *particular solutions* [6,7].

To explain the ability of psychrophilic microorganisms to proliferate at low temperatures (cold adaptation), where natural selection overcomes the problems of protein (cold) unfolding, slow protein folding dynamics, and reduced enzyme activities, a very attractive hypothesis, known as *activity–stability–flexibility* relationships was proposed [6,8]. This hypothesis suggests that psychrophilic proteins might be more flexible than mesophilic and thermophilic homologs, to compensate for reduced kinetic energy at low temperatures. This keeps their atomic fluctuations relatively constant at their corresponding environmental temperature. In this way, researchers proposed that evolution tunes the strength and number of stabilizing interactions that consolidate protein conformations to balance rigidity (for enthalpic stability) and flexibility (for activity) in cold environments [9]. Thus, adaptation to low temperatures would rely on an increase in the intrinsic flexibility of proteins, and this enhancement in flexibility might occur at the expense of a reduction in thermodynamic stability which has been observed for many cold adapted proteins [10–12].

To add more complexity to the scenario, it was also suggested that low stability of cold-adapted proteins may be due to a decrease in selective pressures on thermostability. Moreover, it is not obvious whether a decrease in thermal stability promotes enhanced mobility. *Thus, the relation between thermodynamic stability and flexibility is unclear.*

* Corresponding author. Tel.: +54 11 49648290x108; fax: +54 11 49625457x108.
E-mail address: javiersantosw@gmail.com (J. Santos).

1570-9639/$ – see front matter © 2012 Published by Elsevier B.V.
http://dx.doi.org/10.1016/j.bbapap.2013.02.015

Regarding protein function, an improvement in catalytic efficiency was also observed for many psychrophilic enzymes. Among them, α-amylase of the Antarctic bacterium *Pseudoalteromonas haloplanktis* [8], carbonic anhydrase from the Antarctic teleost *Chionodraco hamatus* [13], and uracil-DNA N-glycosylase [14] were studied. It has been suggested that this fact could be a way to compensate for the lower apparent affinity for ligands at low temperature [6]. Remarkably, the enhanced flexibility may also be reflected by subtle changes in local motions in the catalytic sites or in specific regions that influence the catalytic site architecture [13]. This view, points to the dichotomy between two plausible explanations for cold adaptation of protein function: the existence of an increase in overall flexibility and, on the other hand, enhanced flexibility of only particular stretches of the protein [15]. The latter is also supported by a lack of a direct correlation between enzyme activity and global stability of mutant variants [14].

Flexibility may be considered as a measure of conformational heterogeneity at a given temperature. Mutations that destabilize a protein could decrease their folding constant in such a way that the population of unfolded state increases at a given temperature. However, it has been demonstrated that native states of homolog proteins that are adapted to cold environments can modulate local flexibility without the need of increasing the unfolded state population.

In this way, the thioredoxin of the psychrophilic eubacterium *P. haloplanktis* has an exceptional half-life of 263 min at 95 °C, and higher inactivation kinetics than its mesophilic counterpart [16,17]. In the case of proteins with more complex folding landscapes, partially or locally unfolded states with lower energies compared to the global unfolded state may also contribute to conformational heterogeneity. Regarding the connection between flexibility and conformational heterogeneity, different states can also be populated by flattening of folding energy landscape. This can be achieved with or without a significant change in the free energy of unfolding. For many psychrophilic proteins, the native state has been described as a very heterogeneous ensemble of native conformations with similar conformational stability, yielding fast interconversion between sub-states [18]. The latter can be proposed as a flexibility metrics.

Frataxin (FXN) is a highly conserved protein between species and plays an essential role in iron homeostasis [19], acting as an iron chaperone [20,21]. Although FXN acts as regulatory protein, its biological function differs between eukaryotes and prokaryotes [22]. In the former case, this protein stabilizes the functional form of cysteine desulfurase and Fe–S cluster assembly, whereas in the latter (e.g., CyaY, the FXN homolog in *Escherichia coli*), it abolishes Fe–S cluster synthesis upon binding to the IscS/IscU protein complex. The average native structure of FXN has already been solved by NMR and crystallography [19,23,24] showing an αβ fold with a five-stranded antiparallel β sheet that forms a flat platform and two parallel α-helices that are tightly packed against it, forming an αβ sandwich. Despite differences in the length as the presence of an N-terminal that confers oligomerization properties, and the existence of a variable C-terminal region (CTR) that contributes to enhancing global stability [25], the topologies of FXN homolog proteins are practically superimposable.

To gain insight into the *activity–stability–flexibility* relationships, we focused on FXN of *Psychromonas ingrahamii* (pFXN), an extreme psychrophilic sea-ice bacterium which grows up to −12 °C (generation time of 240 h, strictly psychrophilic: no growth is observed at 15 °C) [26]. In addition, *P. ingrahamii* grows in a wide range of NaCl concentrations (2–18%) and a variable range of pHs (6.5–7.4). [27–29].

Here, we present the pFXN structure and show that the thermodynamic stability of this FXN homolog is significantly reduced and highly modulated by pH, in contrast to other frataxin variants [25]. We also provide structural support for this dependence. Furthermore, we characterize the flexibility of the protein chain and study the role of key interactions in the modulation of pFXN motions by molecular dynamics simulation and computational calculations.

2. Materials and methods

2.1. Protein expression and purification

Frataxin gene from *P. ingrahamii* was synthesized and subcloned into pJexpress411:56977 expression plasmid. Bacteria cultures (*E. coli* BL21 (DE3), 2–3 L 2×YT Broth, pH 7.2) were grown at 37 °C and 280 rpm. Protein expression was induced at DO = 1.0 by addition of 1.0 mM IPTG. After induction for 5 h, bacteria were centrifuged at 6000 rpm and the pellet was stored at −20 °C until cell disruption with French press. Soluble and insoluble fractions were separated by centrifugation at 10,000 rpm (30 min). In this case, both soluble and insoluble fractions contained protein, although, the purity and quantity of pFXN in the insoluble fraction made us continue purification from inclusion bodies. This fraction was resuspended in 50 mL of 10 mM glycine, 6.0 M urea, pH 3.5 (pH was adjusted using phosphoric acid) and incubated for 20 min, at room temperature. After this, the solution was centrifuged at 100,000 *g* and supernatant was transferred to a clean tube. This operation was repeated 3 times. The solution was then carefully loaded onto an ion exchange chromatography (HiTrap SP-HP 5.0 mL column, GE Healthcare), and eluted with a 200 mL linear gradient, from 0.0 to 1.0 M NaCl, in 10 mM glycine, 6.0 M urea, pH 3.5 (this pH was yielded with phosphoric acid). Subsequently, fractions with pFXN identified by SDS-PAGE were neutralized using a 2.0 M Tris–HCl, pH 8.0. The sample was then subjected to exhaustive dialysis against buffer 20 mM Tris–HCl, 100 mM NaCl, pH 7.0. The dialyzed protein was loaded onto preparative Sephadex G-100 column (SEC, 93 cm×2.7 cm), previously equilibrated with the same buffer. This yields >95% pure pFXN; concentration was determined spectroscopically using the extinction coefficient $\varepsilon_{280\ nm} = 16{,}960\ M^{-1}\ cm^{-1}$ ($Abs_{280\ nm}$ 1 mg/mL = 1.38).

2.2. Crystallization, X-ray diffraction, and structure refinement

Crystallization was performed at 24 °C by hanging drop method. One micro-liter of the purified protein at 17.0 mg mL^{-1} (20 mM Tris–HCl, 100 mM NaCl, pH 7.0) was mixed with 1.0 μL of the reservoir solution (200 mM sodium acetate, 200 mM $MgCl_2$, 27.5% polyethylene glycol 4000, pH 4.8). Crystals appeared after 5 days and continued to grow to a maximum size of 300×100×50 μm. They were cryoprotected by transferring them to 200 mM sodium acetate pH 4.8, 200 mM $MgCl_2$, 34% polyethylene glycol 4000 and 5% ethylene glycol and subsequently flash-cooled in liquid nitrogen prior to data collection.

An initial data set was collected at 1.75 Å resolution on the laboratory source. The crystals belonged to the $P2_1$ space group. Data was processed with HKL2000 (Otwinowski and Minor, 1997) and the structure was solved by molecular replacement [30–32] using the Protein Data Bank (PDB) entry 1EW4. A second data set was collected up to a resolution of 1.45 Å on the X06DA beamline at the Swiss Light Source (SLS) (Swistzerland). The structure was refined at 1.45 Å resolution using PHENIX and COOT [33,34], to an R-work = 18.84% and an R-free = 20.05%. Validation tests were done using PHENIX, MolProbit online validation tests, and the ProThe model and PDB validation tests.

Diffraction data has been deposited in the PDB (PDB ID: 4HS5). For data collection and refinement statistics please see Table 1.

2.3. Fluorescence measurements

Steady-state fluorescence measurements were performed in a Jasco FP-6500 spectrofluorometer operating in the ratio mode and equipped with a thermostated cell holder connected to a circulating water bath set at 25 °C. To this end, a 0.3 cm path length cell sealed with a Teflon cap was used. When the intrinsic fluorescence of proteins was measured, excitation wavelength was 295 nm and emission data were collected in the range of 305–430 nm. The spectral slit-width was set to

Please cite this article as: E.A. Roman, et al., Frataxin from *Psychromonas ingrahamii* as a model to study stability modulation within the CyaY protein family, Biochim. Biophys. Acta (2012), http://dx.doi.org/10.1016/j.bbapap.2013.02.015

Table 1
Data collection and refinement statistics. Values in parentheses are for the highest resolution shell.

Data collection	
X-ray source, beamline	SLS, X06DA
Wavelength (Å)	0.9191
Space group (one complex per a.u.)	$P2_1$
Unit-cell parameters	$a=39.84$ Å $b=50.13$ Å $c=45.75$ Å $\beta=91.35$
Resolution range (Å)	31.97–1.45 (1.50–1.45)
No. of observations	107,850
No. of unique reflections	29,948
Multiplicity	3.4 (3.1)
Completeness (%)	97.1 (94.7)
R_{sym} (%)	3.6 (25.5)
Mean $I/\sigma(I)$	26.5 (4.4)
Refinement	
Refinement resolution range (Å)	31.97–1.45
R_{work} (%)	18.84
R_{free} (%)	20.05
No. of reflections for refinement	31,285
Model used for MR	1EW4
$RMSD_{bonds}$ (Å)	0.0063
$RMSD_{angles}$ (°)	1.127
Protein atoms	2032
Water molecules	275
Ramachandran plot favored (%)	98
Ramachandran plot allowed(%)	1
Ramachandran plot outliers (%)	1

3 nm for both monochromators. The percentual contribution of fluorescence at each wavelength ($\%F_\lambda$), for each condition assayed, was calculated as:

$$\%F\lambda = \frac{F\lambda}{Ftotal} \times 100. \quad (1)$$

Quenching experiments were carried out using acrylamide (Sigma) and NaI (Carlo Erba). Ionic strength among samples was maintained constant by the addition of NaCl up to 0.2 M. Moreover, the reducing agent $Na_2S_2O_3$ was added to avoid I_2 production. Excitation was at 295 nm and emission spectra were acquired in the range of 305 to 430 nm. Results were analyzed according to the Stern–Volmer equation:

$$F_0/F = 1 + K_{sv} \times [Q] \quad (2)$$

where F_0 and F are the fluorescence intensities in the absence and presence of quencher, respectively; Q is the quencher concentration and K_{sv} is the collisional quenching constant.

2.4. Circular dichroism spectroscopy

Ellipticity of protein samples was evaluated using a Jasco 810 spectropolarimeter calibrated with (+) 10-camphorsulphonic acid. Far-UV CD spectra were recorded in the range between 200 and 250 nm, protein concentration was 10.0 μM, and a cell of 0.1 cm path-length was used. For near-UV CD spectra, the wavelength range was 250–340 nm, protein concentration was 20 μM, and the path length was 1.0 cm. In all cases, data was acquired at a scan speed of 20 nm min^{-1} and at least 3 scans were averaged for each sample. Blank scans were subtracted from the spectra and values of ellipticity were expressed in units of deg $cm^2 dmol^{-1}$, unless expressed otherwise in the text.

2.5. Protein unfolding experiments

Isothermal unfolding experiments were carried out incubating the pFXN with 0–6.0 M urea in a buffer solution (20 mM phosphate, 100 mM NaCl, 1 mM EDTA) at pHs 6.0, 7.0, and 8.0 for 2 h at room temperature. All measurements were performed at 25 °C. The process was followed by far-UV CD and tryptophan fluorescence measurements. In order to calculate thermodynamic parameters, a two-state unfolding mechanism was assumed, where only native (N) and unfolded (U) conformations exist at equilibrium. Data processing was performed according to Santoro and Bolen [35,36].

Thermal unfolding was monitored by changes in the fluorescence signal of SYPRO orange dye by heating the holder from 4 to 95 °C at a rate of 1 °C min^{-1}. The experiment was performed in a real time PCR system (Biorad). The excitation and emission ranges were 470–500 and 540–700 nm, respectively. Protein concentration was 0.16 mg mL^{-1} and buffer was 20 mM sodium phosphate, whereas the pH range monitored was between 6.0 and 8.0. It is believed that the fluorescence signal is quenched in the aqueous environment but becomes unquenched when binding the apolar core of the protein upon unfolding.

In addition, unfolding transitions as a function of temperature were monitored by the CD signal at 220 nm. Experiments were carried out in 20 mM sodium phosphate, 100 mM NaCl at pHs 6.0, 7.0, and 8.0. Protein concentration was 7.0 μM, and a 1.0 cm cell path length was used. Temperature varied from 10 to 80 °C, at a rate of 1 °C min^{-1}, and the melting curves were sampled at 1 °C intervals. To extract the thermodynamic parameters the following model was fitted to the data:

$$\Delta G_{NU} = -RT\ln\left(\frac{f_U}{f_N}\right) = \Delta H T_m + \Delta C_P(T-T_m) - T\left(\left(\frac{\Delta H T_m}{T_m}\right) + \Delta C_P \ln\left(\frac{T}{T_m}\right)\right) \quad (3)$$

$$S = f_N\left(S_{0,N} + l_N T\right) + f_U\left(S_{0,U} + l_U T\right) \quad (4)$$

where f_U and f_N are the unfolded and folded fractions at equilibrium, respectively; T_m is the temperature at which $f_U = f_N$; S is the observed CD signal; $S_{0,N}$ and $S_{0,U}$ are the intrinsic CD signals for the native and unfolded states, respectively; l_N and l_U are the slopes of the pre- and post-transition regions, respectively, assuming a linear dependence of S_N and S_U with temperature.

2.6. Molecular dynamics simulations. simulation details

2.6.1. Explicit-solvent all atom simulations

To investigate conformational dynamics in the picosecond–nanosecond time scale, we carried out simulations with GROMACS 4.5.5 and GROMOS 53a6 force field [37]. In all cases, the initial structures were generated from the coordinates of the crystallographic structure obtained in this work. The structure of each protein was embedded in a dodecahedral periodic cell with a minimum distance of 0.9 nm between the protein atoms and the cell limits. Both structures were solvated with simple point charge (SPC) water molecules [38]. Sodium and chloride ions were added to shield charges up to 150 mM salt concentration. One thousand steps of energy minimization were performed. After that, 10 ps of protein position restrained simulations were carried out to equilibrate water molecules. A canonical ensemble simulation (N.V.T.) using Berendsen thermostat of 120 ps was performed at 300 K and tau = 0.1 ps^{-1}. Later, microcanonical (N.P.T.) simulation using Berendsen thermostat [39] of 120 ps at 300 K and tau = 1 ps^{-1} was performed [39]. Finally, 500 ps of simulation was performed applying a restraint to alpha carbons (25 kJ mol^{-1}). The resulting structures were the starting points for production simulations (100 ns). For restrained and non-restrained production simulations a Nose–Hoover thermostat was used for temperature coupling, whereas

Please cite this article as: E.A. Roman, et al., Frataxin from *Psychromonas ingrahamii* as a model to study stability modulation within the CyaY protein family, Biochim. Biophys. Acta (2012), http://dx.doi.org/10.1016/j.bbapap.2013.02.015

a Parrinello–Rhaman thermostat was used for pressure coupling. In all cases, long-range interactions were computed according to the particle mesh Ewald method.

3. Results

3.1. Protein expression

The pFXN protein was purified from inclusion bodies in unfolded conditions and refolded from 6.0 M urea by dialysis at 4 °C. The molecular mass obtained by MALDI mass spectrometry (12,284 ± 2) differs in less than 2 Da in comparison with the expected mass deduced from the pFXN amino acid sequence. The purified protein conserves its N-terminal methionine residue. After refolding, the conformation of pFXN protein was studied using spectroscopic and biophysical techniques, including crystallization and X-ray diffraction.

3.2. The crystal structure of Pfxn

To obtain an atomistic description of pFXN structure, crystallization and X-ray diffraction experiments were performed (Table 1 and Fig. 1). The structure of pFXN was solved at 1.45 Å (PDB ID 4HS5). Two protein chains (A and B) occupy the asymmetric unit. Although chains A and B slightly differ in some structural details, including side-chain rotamers, intramolecular interactions [40] (Table 2 and Fig. 1), and B factor values, both chains share the same global topology (backbone RMSD = 1.05 Å). Solving pFXN structure allowed us to accurately explore computationally its flexibility and local stability properties (see below). In Fig. 1A, a structural alignment of FXN homologs that include pFXN, eFXN, and hFXN is shown. FXN structures are almost fully superimposable. It is noteworthy that the psychrophilic variant has a deletion of two residues in loop 1 and a one-residue extension in its C-terminal region (CTR) with respect to eFXN. It should be noted that the pFXN protein has two tryptophan residues (Fig. 1B): one located in the β-sheet region (Trp59), the other (Trp76) in the context of the protein core, interacting with both N- and C-terminal α-helices. In Fig. 1C sequence alignment and the correspondence between the amino acid numbering of different frataxin sequences is shown.

Table 2
Residue interactions within protein chain.

	pFXN 4HS5 (chain A)	pFXN 4HS5 (chain B)	eFXN 1EW4
Hydrophobic interactions within 5 Å	**85**	**87**	**85**
Hydrogen bonds (main chain–main-chain)	**132**	**143**	**129**
Hydrogen bonds (main chain–side-chain)	**43**	**33**	**33**
Hydrogen bonds (side chain–side-chain)	**55**	**56**	**50**
Hydrogen bonds (total)	**230**	**232**	**212**
Ionic interactions within 6 Å	**9**	**7**	**8**
Aromatic–aromatic with in 4.5 Å	**4**	**4**	**6**
Aromatic–sulfur with in 5.5 Å	**0**	**0**	**1**
Cation-pi within 6 Å	**3**	**1**	**3**

Interactions were calculated using the server PIC (protein interactions calculator), Molecular Biophysics Unit, Indian Institute of Science, Bangalore [40].

3.3. Spectroscopic characterization

3.3.1. Native state signatures

To evaluate whether pFXN protein acquires a native structure in aqueous solution, CD spectroscopy was used. Circular dichroism spectrum in the far UV region (far-UV CD) provided information on the secondary structure content of a protein. The spectrum of pFXN at 25 °C showed the classical signatures of a well folded protein (Fig. 2A). Major contributions occurred at 208 and 220 nm. This result indicates that N- and C-terminal α-helices are consolidated. To study the tertiary structure of this protein, ellipticity in the near-UV region, at 25 °C, was also evaluated. Near-UV CD spectrum showed signatures of a properly-folded protein (Fig. 2B). The region involving aromatic residues between 280 and 295 nm had strong differential absorption, which showed that the contributing amino acid residues are well packed. Also, the fourth derivative of the UV-absorption spectra showed that aromatic amino acid residues are preponderantly located in a hydrophobic environment, which is compatible with tryptophan in a buried

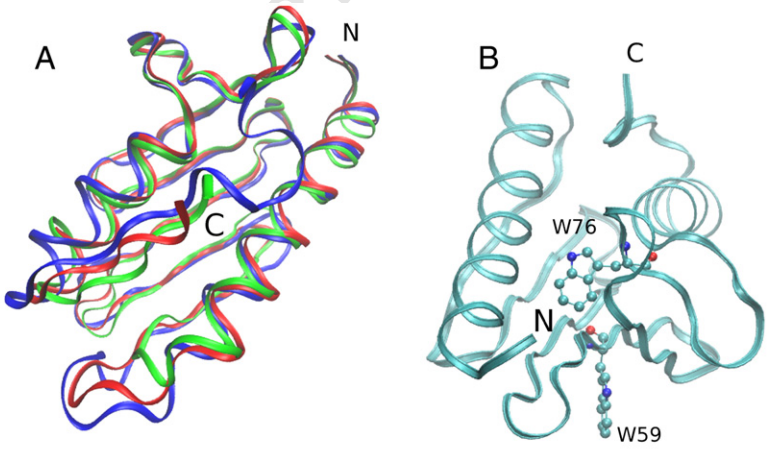

C

```
hFXN  90  LDETTYERLA EETLDSLAEF FEDLADKPYT FEDYDVSFGS GVLTVKLGGD GTYVINKQTP 149
eFXN   1  MNDSEFHRLA DQLWLTIEER LDDWD----G DSDIDCEING GVLTITFENG SKIIINRQEP  56
pFXN   1  MNDSEFIQLA DQLYQKIEEK IEESG----- -ADVDYDQNG SLLTLEFENH TKLIINRQQP  54

hFXN 150  NKQIWLSSPS SGPKRYDWTG KNWVYSHDGV SLHELLAAEL TKALKTKLDL SSLAYSGK   208
eFXN  57  LHQVWLATKQ G-GYHFDLKG DEWICDRSGE TFWDLLEQAA TQQAGETVSF R-------   106
pFXN  55  LHQVWLATLE N-GHHYDYNN GKWIDDRSGD EFLTFLSAAI FKQSKETVDF TE------   105
```

Fig. 1. The structure of pFXN. A) Structural alignment of FXN homologs that include pFXN (green), eFXN (red), and hFXN (blue) is shown in ribbon representation. B) Two Trp residues of pFXN: Trp59 is located in the β-sheet region and Trp76 is in the core of the protein. C) Sequence alignment and correspondence between amino acid numbering in different frataxin sequences.

Please cite this article as: E.A. Roman, et al., Frataxin from *Psychromonas ingrahamii* as a model to study stability modulation within the CyaY protein family, Biochim. Biophys. Acta (2012), http://dx.doi.org/10.1016/j.bbapap.2013.02.015

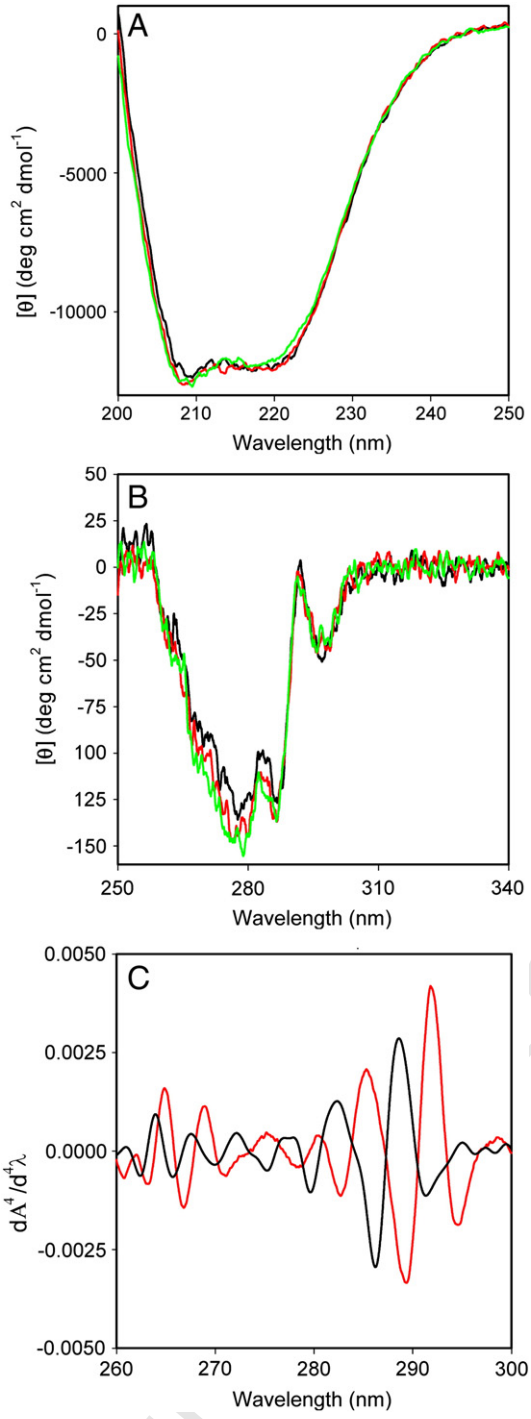

Fig. 2. Circular dichroism and UV-absorption signals from native conformations of pFXN. A) Molar ellipticity of pFXN between 250 nm and 200 nm is plotted at pH 6.0 (black line), pH 7.0 (red line), and pH 8.0 (green line). B) Molar ellipticity of pFXN between 340 nm and 250 nm is plotted at pH 6.0 (black line), pH 7.0 (red line), and pH 8.0 (green line). C) Fourth-derivative of the UV spectra of pFXN protein. Ultraviolet absorption in the region between 250 nm and 320 nm was collected and the average spectrum was derived four times with respect to the wavelength. The fourth derivative of the absorption spectrum of N-acetyl tryptophan amide is shown in red as a reference of the absorption from polar environments, and the fourth derivative of pFXN absorption is in black.

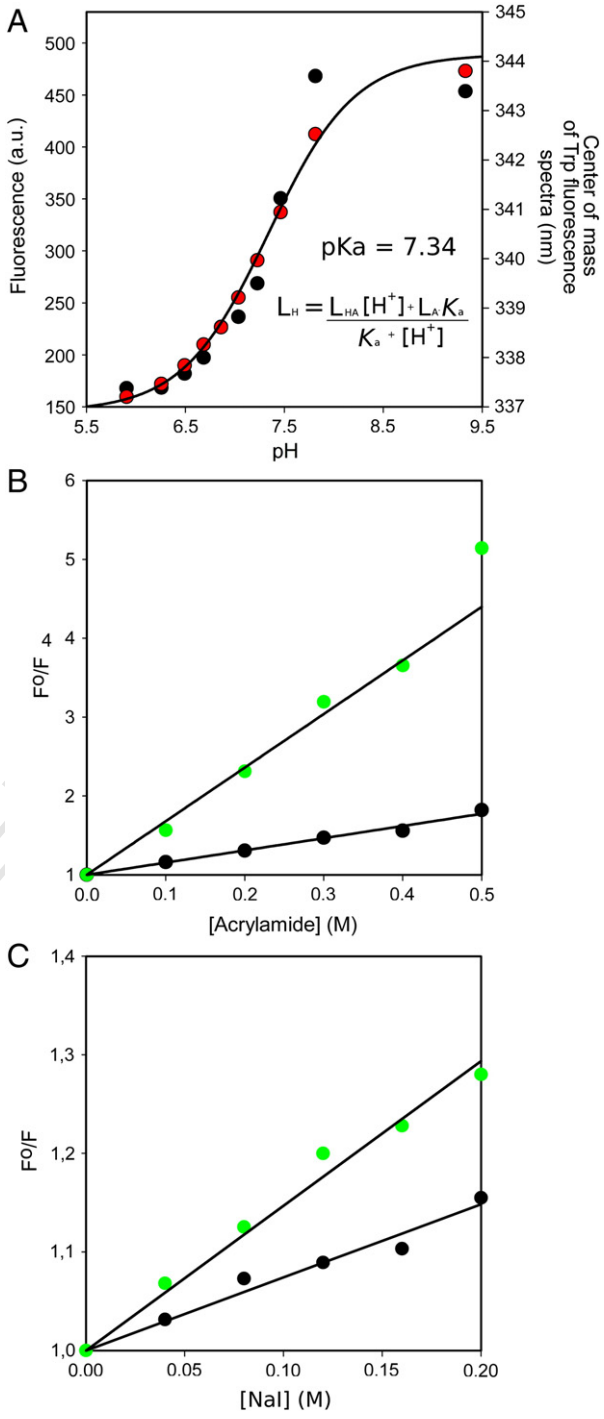

Fig. 3. Effect of pH on native Trp fluorescence of pFXN. A) Fluorescence at 350 nm (black symbols) and the center of spectral mass of Trp emission (red symbols) were plotted as a function of pH. The solid line represents the fitting of equation $L_{(H)} = (L_{(HA)} \times [H^+] + L_{(A-)} \times K_a)/(K_a + [H^+])$ to the data [57]. $L_{(H)}$ is the total fluorescence signal at pH = H, $L_{(HA)}$ and $L_{(A-)}$ are the fluorescence signals corresponding to the protonated and deprotonated forms at pH = H, *Ka* referrers to the apparent constant for the transition observed, and $[H^+]$ is the proton concentration. Stern–Volmer plots for the quenching of Trp fluorescence by acrylamide (B) and sodium iodide (C), both at pH 6.0 and pH 8.0 (black and green symbols, respectively). The Trp fluorescence Stern–Volmer constants for acrylamide were $K_{sv-pH6.0} = 1.56 \pm 0.09$ and $K_{sv-pH8.0} = 7.96 \pm 0.19\ M^{-1}$, while for sodium iodide were $K_{sv-pH6.0} = 0.72 \pm 0.06$ and $K_{sv-pH8.0} = 1.40 \pm 0.08\ M^{-1}$. Tryptophan fluorescence was measured by excitation at 295 nm and emission was collected between 305 nm and 430 nm.

conformation (inaccessible to the solvent) and a compact native structure (Fig. 2C). Thus, the refolded protein has a native-like structure.

To gain more insight into the tertiary structure of pFXN, we measured its tryptophan fluorescence. The spectrum of the native protein has a center of spectral mass of ~337 nm at pH 7.0 (Figs. 3A and S1). This value is in agreement with emissions from an apolar environment.

3.3.2. Effect of pH on native state signatures

As Trp59 is interacting with His68 (see below, Fig. 7B and E), we thought that the nature of this interaction may be modulating protein

Please cite this article as: E.A. Roman, et al., Frataxin from *Psychromonas ingrahamii* as a model to study stability modulation within the CyaY protein family, Biochim. Biophys. Acta (2012), http://dx.doi.org/10.1016/j.bbapap.2013.02.015

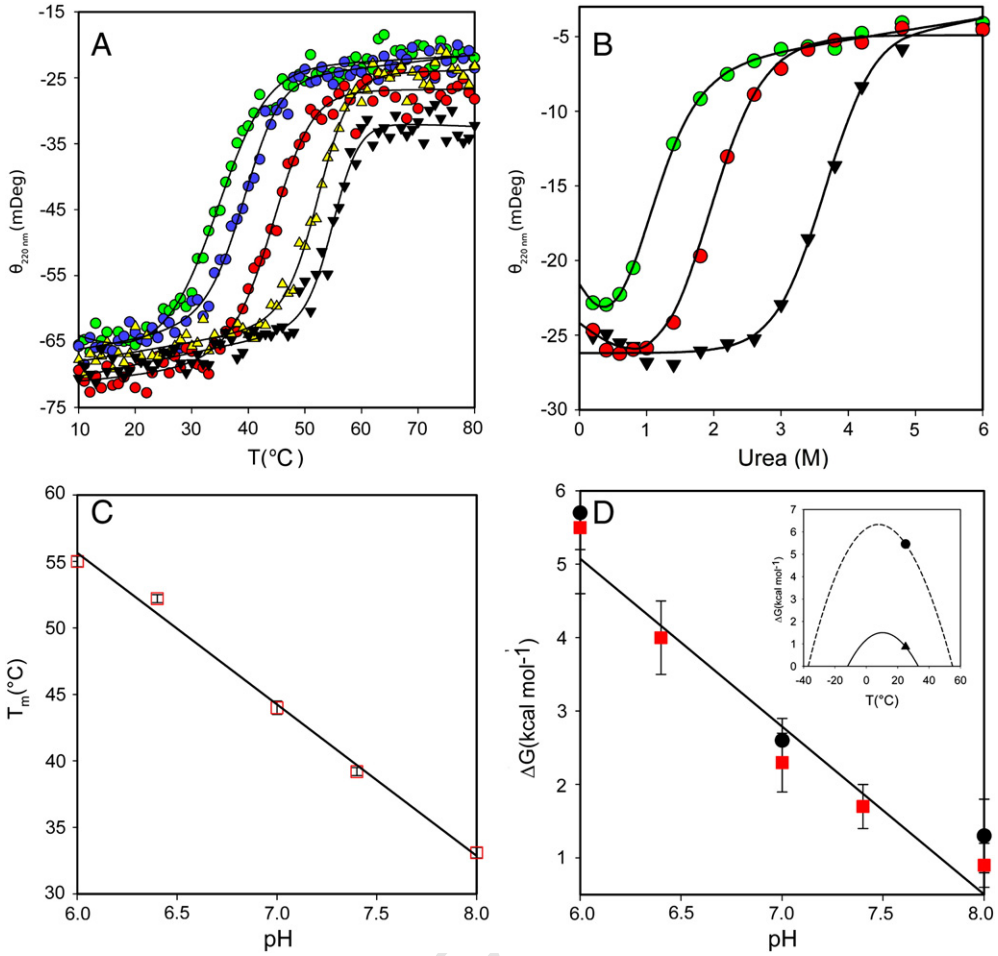

Fig. 4. Unfolding of pFXN followed by circular dichroism. A) pFXN was heated from 10 °C up to 80 °C at a rate of 1 °C min^{-1}, at pH 8.0 (black symbols), pH 7.4 (red symbols), pH 7.0 (green symbols), pH 6.4 (yellow symbols), and pH 6.0 (blue symbols). Ellipticity at 220 nm was collected and plotted as a function of temperature. B) pFXN was incubated for 2 h (25 °C) at different urea concentrations, in buffer at pH 8.0 (black symbols), pH 7.0 (red symbols), or pH 6.0 (green symbols). Ellipticity at 220 nm was plotted as a function of urea concentration. C) Melting temperature was extracted from Fig. 3A and plotted as a function of pH in square symbols. D) Free energy of unfolding at 25 °C as a function of pH. Black symbols represent ΔG_{NU} calculated in urea-unfolding experiments, while red points are ΔG_{NU} at 25 °C calculated from temperature unfolding experiments. In all cases vertical bars represent experimental values ± SD, whereas the black line represents their tendency. The inset shows ΔG_{NU} as a function of temperature, at different pH values (solid line: pH 8.0, dashed line: pH 6.0). Symbols in the inset represent ΔG_{NU} at 25 °C.

conformation by modifying the Trp59 environment. Therefore, protonation state of His68 might have a role in pFXN structure consolidation. As a consequence, we decided to study spectroscopic signatures in the range of pH around the p*K*a of histidine, which is around most common physiological pHs. Dependence of ellipticity between pH 6.0 and 8.0 was studied. Both far- and near-UV CD spectra do not vary their overall values within this range, at 25 °C (Fig. 2A and B). This fact evidences that there are no major structural changes in the native state upon pH shift.

Next, the effect of pH in tryptophan fluorescence (Fig. 3A) was measured. We found that as it increases from 6.0 to 8.0, the center of spectral mass of Trp fluorescence shifts from ~337 to ~341 nm (Fig. 3A), and also fluorescence intensity increased in a cooperative fashion (Fig. 3A). This is in agreement with crystallographic data which showed that His68 could be a good quencher of Trp59 since these residues are at ~3.5 Å at an optimal geometry for a π–cation interaction. This interaction seems to have the ability to shift between π−π and π–cation (when histidine side-chain is positively charged), depending on the pH of the media. It is worthy of note that at pH 8.0, the quenching efficiency is significantly decreased. In the same fashion, it was previously reported that neutral His residues are less efficient as quenchers compared to positively charged ones [41]. On the other hand, the second tryptophan residue, Trp76 has two potential quenchers, Tyr69 and Tyr71, but they are more than 4 Å away. In addition, these residues do not seem to be in a good geometry to interact with Trp76. Furthermore, a close look at the crystal structure shows three water molecules at ~3 Å of Trp76 which can explain the poor contribution of this residue to native fluorescence (Fig. S1). Consequently, our analysis suggests that the changes in fluorescence intensity and wavelength shift upon increasing the pH from 6.0 to 8.0 would more likely come from an alteration of the local chemical environment of Trp59.

Remarkably, quenching of Trp fluorescence by acrylamide is enhanced at pH 8.0 (Fig. 3B). More likely, this is due to the presence of a less stable and more dynamic protein structure in this condition. It is worth noting that acrylamide is a neutral molecule that is more able to access to the core of the protein and quench buried Trp residues. A different picture is observed using sodium iodide (Fig. 3C), a polar quencher with less penetration capability. Although quenching by iodide is also observed in the range of pH 6 to pH 8 (Fig. 3C), at pH 8.0 the Stern–Volmer constant for iodide is significantly lower than acrylamide, probably, at least in part, due to the charged nature of this ion, in addition to its size. Even taking into account that efficiency is different for each of the quenchers [42], accessibility of acrylamide and iodide at pH 8.0 is still considerably different. Thus, these results show that Trp residues are more accessible at this pH.

Please cite this article as: E.A. Roman, et al., Frataxin from *Psychromonas ingrahamii* as a model to study stability modulation within the CyaY protein family, Biochim. Biophys. Acta (2012), http://dx.doi.org/10.1016/j.bbapap.2013.02.015

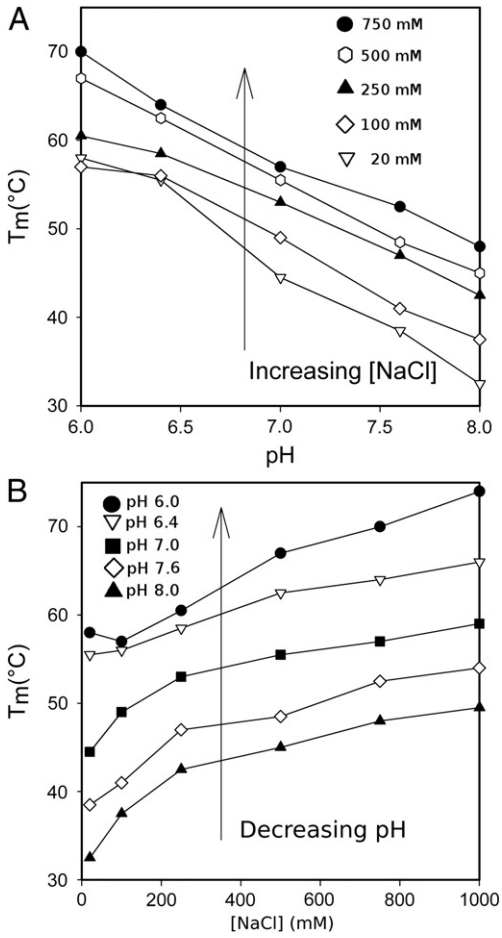

Fig. 5. Melting temperature of pFXN monitored by SYPRO orange probe. A) Effect of pH on the T_m, at different NaCl concentrations: 20 mM (white triangles), 100 mM (white diamonds), 250 mM (black triangles), 500 mM (white hexagons), and 1000 mM (black circles). B) Effect of NaCl concentrations on melting T_m, at different pH values: 6.0 (black circles), 6.4 (white triangles), 7.0 (black squares), 7.6 (white diamonds), and 8.0 (black triangles).

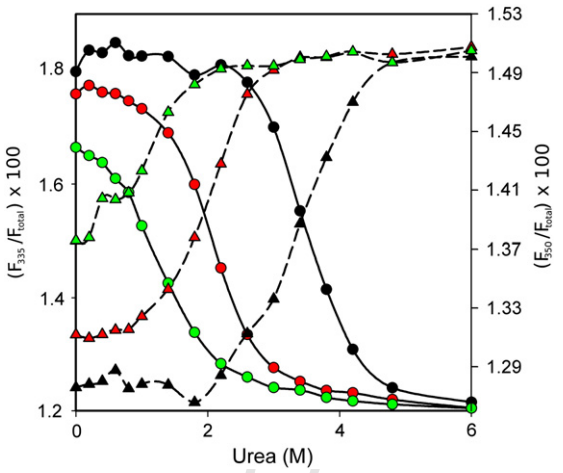

Fig. 6. Fluorescence change at 335 nm and 350 nm relative to total tryptophan fluorescence emission. Solid lines account for a change in emission at 335 nm, while dashed lines show a change in emission at 350 nm. Black symbols are the values obtained at pH 6.0, red symbols are the ones obtained at pH 7.0, and green symbols are the ones obtained at pH 8.0.

However, these amino acids are still moderately buried since iodide is not able to fully quench Trp residues (in agreement with the maximum emission wavelength observed, see Fig. 3).

3.3.3. Effect of the pH and ionic strength in pFXN stability

3.3.3.1. Thermal unfolding. Thermal unfolding experiments were performed to study the thermodynamic stability of pFXN. In Fig. 4A we show the reversible change in ellipticity at 220 nm upon heating pFXN protein at 1.0 °C min^{-1}. As can be seen, melting temperature (T_m) is strongly dependent on pH. At pH 6.0, T_m reaches a value of 55 °C. However, as the buffer becomes more alkaline, the T_m value shifts to 32 °C (at pH 8.0). This substantial difference in T_m (~20 °C) indicates that at pH 8.0 the protein is considerably less stable compared with pH 6.0 (Fig. 4A). As the transition was >90% reversible at all pHs assayed, thermodynamic characterization of the unfolding reaction was performed (Table 3). At pH 6.0, the pFXN protein is ~5 kcal/mol more stable compared to pH 8.0. This suggests that, within this range of pH, the charge and protonation state of the protein might be modulating its global stability (Fig. 4). The free-energy dependence on temperature was also calculated from thermal denaturation experiments and plotted (Fig. 4C, inset and Table 3). As the protein became more stable, the cold-unfolding temperature (T_C) also shifted to lower values. Further experiments using DSC should be performed to gain specific information.

In addition, we tested the effect of pH on fluorescence of SYPRO orange, which is a fluorescent probe that binds to the unfolded state of proteins [43–45]. Hence, unfolding can be studied by following the abrupt increase in fluorescence when the protein reaches its T_m. In accordance to CD experiments, where unfolding is followed by a reduction in the CD band (220 nm), a decrease from pH 8.0 to 6.0 yielded a shift of the transition to higher temperatures, an indication of protein stabilization (Figs. 5 and S2). Moreover, the effect of NaCl concentration was also assessed. Previous results for the human, yeast and *E. coli* variants showed that the addition of salts increased the stability of the FXN. To evaluate whether this characteristic is shared by pFXN, we monitored the effect of ionic strength on protein stability by measuring the dependence of the T_m on NaCl concentration (Fig. 5). The incubation of pFXN with NaCl in the range of zero to 1.0 M yields an increase in the T_m. The same tendency was observed at all tested pHs (Fig. 5). The result suggests that salt- and pH-induced stabilization effects are independent. This might be a consequence of local stabilization in different regions of the protein: we hypothesize that ionic strength may stabilize the Asp/Glu rich regions, as in the case of *E. coli* and the human variants [25], whereas a decrease in pHs from 8.0 to 6.0 would exert its influence by modulation of the protonation state of histidine residues and their involvement in an interaction network. Therefore, a fine balance between both pH and salt concentrations could tune function and stability of pFXN. Further comments will be made in the Discussion section.

3.3.3.2. Chemical unfolding. To further investigate the effect of pH on thermodynamic stability we performed urea-unfolding experiments, following changes in protein conformation by both CD at 220 nm and tryptophan fluorescence. In Fig. 6, the contribution of fluorescence at 335 and 350 nm at each urea concentration is plotted. At every pH, the contribution of 335 nm decreases as urea concentration increases; the opposite occurs for 350 nm. This indicates that when denaturant concentration increases, the tryptophan residues are less quenched (increase in fluorescence intensity) and in a more polar environment (shift towards λ_{350}), comparing with the native state (Fig. S1).

When unfolding was followed by CD signal at 220 nm, a similar tendency was observed for each pH value (Fig. 4B). The denaturation transition observed superimposes with the one observed by Trp fluorescence ratio 335/350 nm (Fig. S3). Thus, the change in fluorescence upon unfolding is accompanied by a change in secondary structure content. Values of $\Delta G^{\circ}_{NU\ H_2O}$ for urea unfolding are plotted in Fig. 4D

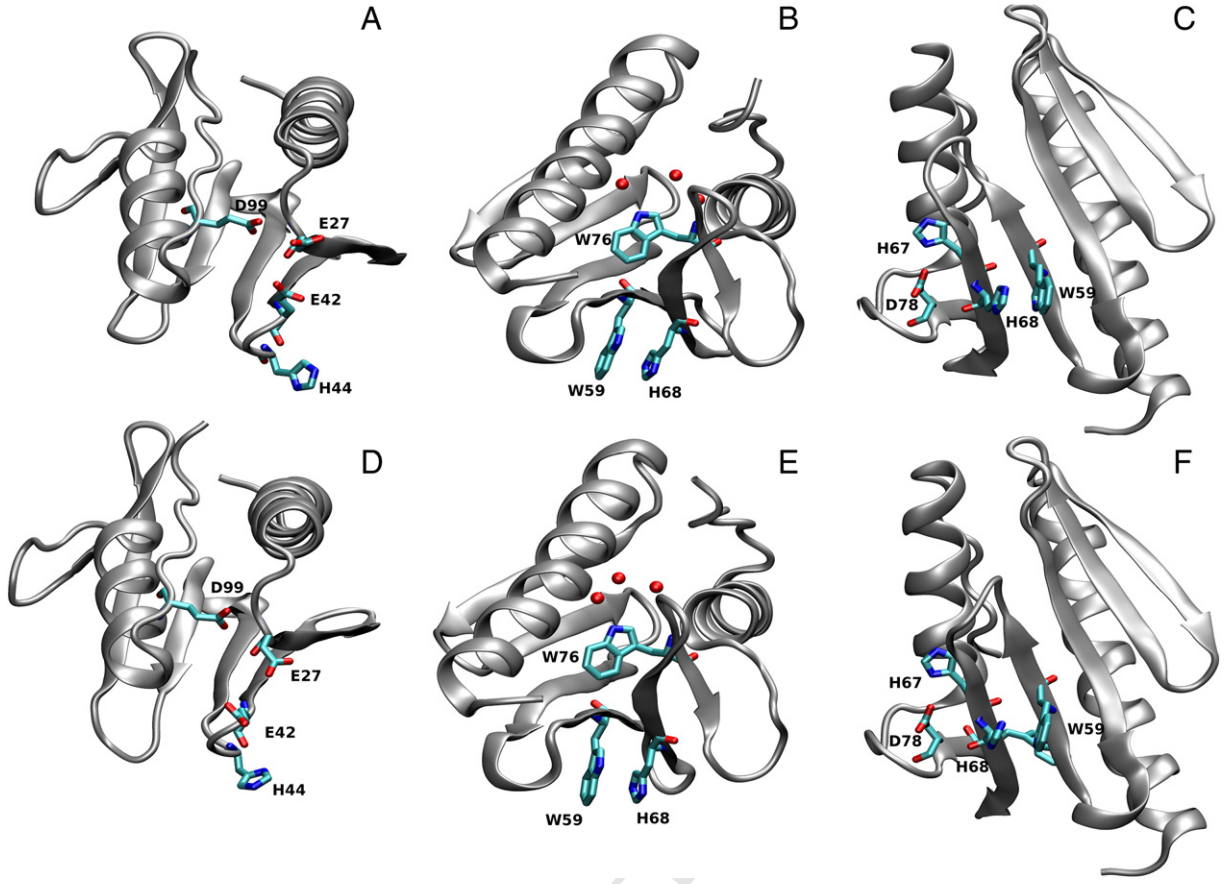

Fig. 7. Interactions involving histidine residues in pFXN structure. Chains A (panels A, B, and C) and B (panels D, E, and F) of the crystallographic unit cell are represented. A and D) Electrostatic network formed between residues D99, E27, E42, and H44. B and E) Tryptophan residues in pFXN. W59 interacts with H68, while W76 interacts with three water molecules at less than 3.5 Å. C and F) Histidine 67 and 68 interactions. H67 forms ionic interaction with D78, while H68 forms π–cation interaction with W59.

and summarized in Table 4. Briefly, the dependence of stability is $\Delta G^{\circ}_{NU\ H_2O\ pH6} > \Delta G^{\circ}_{NU\ H_2O\ pH7} > \Delta G^{\circ}_{NU\ H_2O\ pH8}$.

We think that the strength of some interactions present in the native state could be coupled to the pH shift, modulating not only the stability of the protein but also the conformational heterogeneity of the native ensemble.

3.3.4. Computational analysis of pFXN structure

3.3.4.1. Local stability. To analyze pFXN structure in terms of local stabilities, we performed COREX calculations [46,47]. In Fig. 8A and B, the relative stability is plotted as a function of the residue number. It can be seen that for both pFXN and *E. coli* variant (eFXN) there are differences between their stability profiles. In the case of eFXN, the loops between strands β2/β3 and β5/β6 are the less stable ones. However, residues 60–70 in pFXN (the loop between β4/β5) show a major probability of experiencing local unfolding. It is important to remark that for residues 62–66 (chain B), B-factors are the highest in pFXN and eFXN crystal structures. This result points to this region as being highly flexible.

In addition, to evaluate energy contribution per residue to global stability we performed FOLDX calculations for both variants [48]. In particular, we performed the *alanine scan* protocol to uncover residues contributing to destabilization of the native protein, comparing them with their corresponding alanine point mutant (Fig. S4A). Among these residues, Asp11, Glu18, Glu19, Glu23, Asp27, Asp29, Asp31, Glu42, Asp70, Asp78, Asp79, Asp83, Glu99 and Glu105 have acidic side-chains. It is noteworthy that 14 out of the 21 Glu/Asp residues of the pFXN protein are destabilizing. In the same fashion,

Table 3
Temperature unfolding of pFXN followed by far-UV CD at 220 nm.

Two state model fitting (N ↔ U). Temperature unfolding			
Circular dichroism			
pFXN	ΔH_{NU} (kcal mol^{-1})	T_m (°C)	ΔG_{NU} at 25 °C (kcal mol^{-1})
pH 6.0	85.7 ± 10	55.0 ± 0.4	5.5 ± 0.9
pH 6.4	71.3 ± 6	52.2 ± 0.3	4.0 ± 0.5
pH 7.0	54.1 ± 6	44.0 ± 0.5	2.3 ± 0.4
pH 7.4	50.2 ± 3	39.2 ± 0.3	1.7 ± 0.3
pH 8.0	39.8 ± 6	33.1 ± 1.0	0.9 ± 0.3[a]

[a] It should be noted that the difference in heat capacity between native and unfolded states ($\Delta C_{P\ NU}$) was considered unchanged ($\Delta C_{P\ NU} = 1.68$ kcal mol^{-1} K^{-1}) upon changes in pH, since native and denatured signals were similar in CD experiments. Its value was fixed taking into account the empirical relation between the length of the protein and the difference of the solvent accessible surface area between native and unfolded states (ΔASA_{NU}) [59].

Table 4
Chemical unfolding of pFXN followed by far-UV CD at 220 nm.

Two state model fitting (N ↔ U). Urea unfolding					
Circular dichroism					
pFXN	$\Delta G^{\circ}_{NU\ (H_2O)}$ (kcal mol^{-1})	m_{NU} (kcal mol^{-1} M^{-1})	$C_{m\ NU}$ (M)	S^0_N (mdeg)	S^0_U (mdeg)
pH 6.0	5.7 ± 0.5	1.57 ± 0.2	3.6 ± 0.6	−26.2 ± 0.2	−6.6 ± 4
pH 7.0	2.6 ± 0.3	1.42 ± 0.1	1.8 ± 0.2	−24.4 ± 0.4	−4.9 ± 0.2
pH 8.0	1.3 ± 0.5	1.62 ± 0.2	0.8 ± 0.3	−23.0 ± 0.7	−8.1 ± 0.6

Please cite this article as: E.A. Roman, et al., Frataxin from *Psychromonas ingrahamii* as a model to study stability modulation within the CyaY protein family, Biochim. Biophys. Acta (2012), http://dx.doi.org/10.1016/j.bbapap.2013.02.015

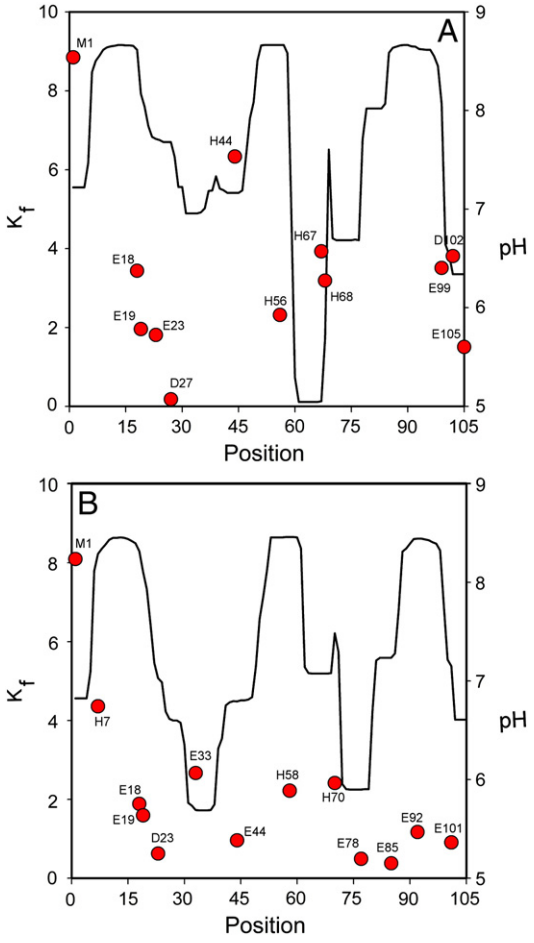

Fig. 8. Computational calculations using pFXN-solved structure. Folding constant per residue as calculated by COREX online software (left axis), and the p*K*a values of residues as calculated by Bluues Server (red dots, right axis) for A) pFXN and B) eFXN.

Correia et al. [49] documented in detail the stabilizing effect produced by mutation of acidic side-chains in the acidic ridge region. In this case, the multiple mutant D86A/E90A/E93A/D101A/E103A of yeast FXN (yFXN) is stabilized at ~3 kcal compared to wild-type protein.

In addition, Lys20, Gln32, Ser35, Thr62, and Gly66, Asn72, Ser90, Gly93, Phe94 and Lys98 are also destabilizing. The same procedure was performed for the crystal structure of *E. coli* variant (PDB ID: 1EW4). The alanine substitution energy profile was similar. However, when we analyzed the differences at each position in the sequence alignment, the destabilization effect of point mutation was greater for eFXN (Fig. S4B).

3.3.4.2. Distribution of predicted pKa values in the protein. As the stability of pFXN is modulated by pHs between 6.0 and 8.0, and given that this does not occur for eFXN, the p*K*a value of the ionizable residues would aid in the understanding of the mechanism involved in protein stabilization. To evaluate which residues may contribute, we calculated p*K*a values by using the crystal structures of *E. coli* (PDB ID: 1EW4) and *P. ingrahamii* variants (PDB ID 4HS5). Calculations were made with the Bluues server from Silvio Tosatto's laboratory (http://biocomp.bio.unipd.it/bluues) [50]. Fig. 8A and B shows the residues with a predicted p*K*a value between pH 6.0 and pH 8.0. It can be seen that only two residues are included within this range for the eFXN (in the N-terminal). However, there are nine candidates (Glu18, Glu19, Glu23, His44, His56, His67, His68, Glu99, Asp102) in pFXN. Most of these residues are located in regions of reduced local stability, as predicted by COREX. It is worth noting that p*K*a values strongly depend on fine details of side-chain packing, protein–solvent interactions, and molecular dynamics; thus, our calculations are indicative predictions of putative regions that might be related to the dependence of stability on pH. However, altogether, these results suggest that the electrostatic network formed by some of these residues in pFXN may play an important role in local stability modulation.

3.3.5. Flexibility distribution in the protein

3.3.5.1. B-factor analysis and molecular dynamics simulations. Protein regions that exhibit high mobility due to thermal motions usually show a broadening in the electron density map, which is called *temperature factors* or *B-factors*. In Fig. 9 a comparison between relative B-factors of chains A and B of pFXN (1.45 Å) and the single chain of eFXN (1.40 Å) is shown. Although global features in the localization of high B-factor values are shared in both proteins, patches corresponding to the highest values differ between homologs. This may indicate that the distribution of flexibility in the protein chain is also different.

More importantly, in pFXN, residues 62–66 (the turn between strand β4 and strand β5) in chain B show the highest relative B-factor values observed in both structures. In fact, in the structure solved at 1.75 Å, the electron density corresponding to this stretch is inexistent (data not shown). This observation points to a crucial difference in flexibility when comparing pFXN to *E. coli* homolog. However, eFXN structure has delimited patches (Arg20-Ser28 and Leu73-Asp76) of high B-factors compared with pFXN. Remarkably, NMR structure of the *E. coli* variant (PDB ID: 1SOY) shows a high RMSD between models in region Arg20 to Ser28, more likely indicating an increased flexibility within these stretches. Although relative B-factors observed for strand β1/loop1 for pFXN are lower than values for eFXN, this region is included in an extensive segment with intermediate values of B factors, in particular, in chain A (residues Lys20-Leu36), also suggesting smooth differences in which flexibility maps throughout the protein chain.

In addition, the C-terminal region (CTR) involving residues Gln96-Asp102 (including Glu99) shows significantly higher values in the case of pFXN (chains A and B) than in *E. coli* homolog. Mobility in this region might be associated to both local and global dynamics, since this region is implicated in the thermodynamic stabilization of FXN fold [51].

To evaluate the mobility of the chain for both homologs at the atomic level, we performed all-atom MDS (Figs. 9 and S5). After 100 ns of computational simulation, both proteins have similar root mean square deviations (RMSD, Fig. S5). Remarkably, there is a general superimposition between regions with high B-factors and higher root mean square fluctuations (RMSF, Fig. 9), indicating a correlation

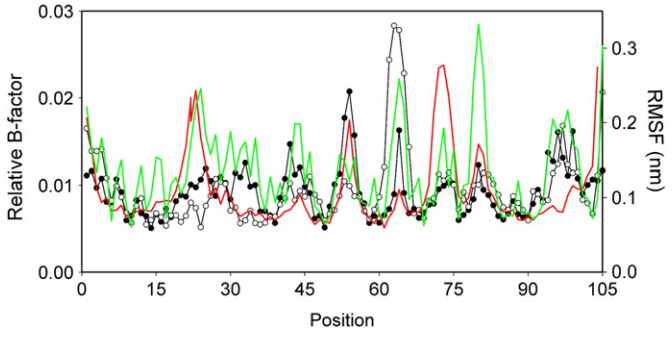

Fig. 9. Flexibility of pFXN structure: a comparison between crystallographic B-factor values and root mean square fluctuations (RMSF) calculated by MDS. In black and white dots, the B-factors of chains A and B of pFXN are represented, respectively. The red line accounts for the B-factors in the *E. coli* structure. The green line represents the RMSF as calculated from 100 ns by molecular dynamics simulations of pFXN (right axis). The relative B-factor was calculated as a ratio of the B-factor at each position divided by the sum of the whole B-factor values.

Please cite this article as: E.A. Roman, et al., Frataxin from *Psychromonas ingrahamii* as a model to study stability modulation within the CyaY protein family, Biochim. Biophys. Acta (2012), http://dx.doi.org/10.1016/j.bbapap.2013.02.015

between experimental and in silico results. Curiously, the main difference between both variants occurs at the CTR, which has higher RMSF values in the case of pFXN.

3.3.5.2. Analysis of specific motions in pFXN. To see whether the protonation state of histidine residues is involved in pFXN motions we performed two extra MDS runs where His44 or His67 were in their protonated form. Both RMSD and RMSF are described in Fig. 10A and B. In both cases, it can be seen that the individual protonation of these residues reduced the mobility of segments 20–30 and 90–100, suggesting that the fluctuations of these regions are correlated.

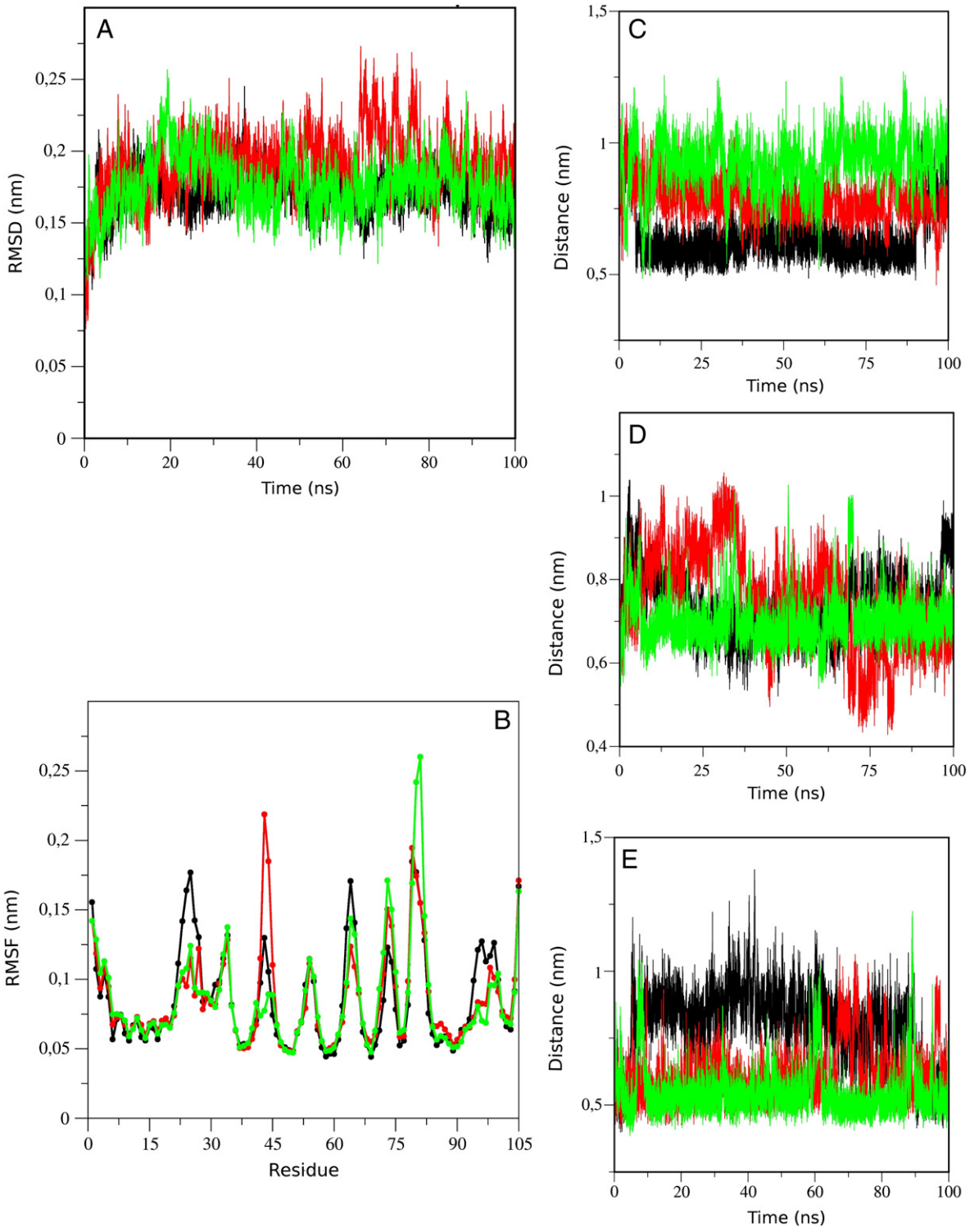

Fig. 10. Molecular dynamics simulations of pFXN. A) Black lines represent the root mean square deviations (RMSD) of pFXN with histidine residues uncharged. Red and green lines represent pFXN with protonated His67 and protonated His44, respectively. B) Black lines represent RMSF of pFXN with histidine residues uncharged. Red and green lines account for pFXN with protonated His67 and protonated His44, respectively. C), D), and E) Distances between Asp27 and Glu99, Glu42 and Asp27, and His44 and Glu42 were represented, for the three variants simulated, respectively.

Please cite this article as: E.A. Roman, et al., Frataxin from *Psychromonas ingrahamii* as a model to study stability modulation within the CyaY protein family, Biochim. Biophys. Acta (2012), http://dx.doi.org/10.1016/j.bbapap.2013.02.015

As mentioned before, residues Asp27, His44, Glu42 and Glu99 establish tertiary contacts between loop1 and the CTR. For this reason, and given the high RMSF for these residues, we searched for correlations between motions involved in the interaction network formed by these amino acids (Fig. 10C, D and E). We observed that the C-extreme of helix α1, including Glu23, unfolds locally and refolds. Noteworthy, when His44 or His67 are protonated, both loop 1 (encompassing residues 25–30) and the C-terminal become closer to each other.

Altogether, we think that the electrostatic network formed between acidic residues connecting N- and C-extremes, including water molecules, may be modulating stability and dynamics. Binding of metal ions might further affect the flexibility of this region.

4. Discussion

In cold environments, macromolecular motions involved in enzyme catalysis, binding interactions, and cellular homeostasis need to occur under conditions where kinetic energy is lower compared to warm and hot environments. In particular, FXN seems to be involved in a multiplicity of processes [52–56]. The most explored of which correspond to iron binding and metal ion exchange, as well as those that situate FXN as a key regulator component in iron/sulfur center synthesis. Both kinds of processes take place via metal protein-ion/protein–protein interactions. Thus, adaptation mechanisms may be identifiable and used, for example, in protein and drug designs.

The X-ray diffraction results included here show that pFXN shares the same structural topology with other members of the CyaY protein family. In particular, the FXN homolog from *E. coli* has been an interesting study case [25]. Both pFXN and eFXN share ~51% of their sequence identity. However, differences at specific positions exist and could act as modulators of stability or/and flexibility. In this sense, although they share the acidic ridge region, content and distribution of glutamate, aspartate, asparagine, and glutamine slightly differ between both variants. It is noteworthy that the content of Asn and Gln in proteins from organisms adapted to cold environments increases since the likelihood of deamidation is lower at these temperatures [26]. For the case of Gln and Asn (15 in pFXN versus 11 in eFXN), pFXN has four of these residues along its N-terminal α-helix, whereas eFXN has only two. Moreover, eFXN has three of these in the C-terminal α-helix, while pFXN has only one in this region. We cannot rule out that Gln and Asn might play a role in metal binding within the acidic ridge region. In the case of acidic side-chains, which are crucial for biological function, there are 21 in pFXN versus 22 in eFXN. Yet, pFXN Glu and Asp content in the N-terminal α-helix is five and two, respectively, (Glu to Asp ratio of 2.5), whereas for eFXN Glu content is three and Asp content is five (Glu to Asp ratio of 0.6). The increase in the side-chain length might play a role in the coupling between local flexibility and function.

Recently, we have shown a key role of the CTR in determining the global stability of the human variant [51]. In the present case, pFXN and eFXN share almost the same CTR length (7 and 8 residues, respectively) being shorter than the human variant (16 residues). However, the CTR of eFXN and pFXN differ significantly in sequence. In fact, pFXN has multiple acidic side-chains that may be implicated in metal ion binding (Glu99, Asp102 and Glu105) whereas eFXN has only one (Glu101). Results from our laboratory are in agreement with this possibility as seen in preliminary X-ray structures where metal ions are coordinated by Asp102 and Glu105 (data not shown). On the other hand, both proteins have hydrophobic residues in the CTR that anchor this region to the rest of the protein (Val101 and Phe103 from pFXN superimposes to Val103 and Phe105 from eFXN).

Regarding thermodynamic analysis of chemical and temperature unfolding experiments, pFXN is much less stable than eFXN, and its stability is highly modulated by pH in the range of 6.0–8.0. The unfolding at pH 7.0 for pFXN in comparison to eFXN [25] yields a lower T_m value (ΔT_m ~10 °C). However, when pH is shifted to pH 8.0, T_m of pFXN experiences a larger decrease (ΔT_m ~20 °C). On the other hand, the acidification of buffer to pH 6.0 increases the T_m (Table 3) to similar values as the ones observed for eFXN [25]. Notably, our spectroscopic results demonstrate that, although global conformational features of the native ensemble do not change along the range of pH tested (Figs. 2 and 3), some local variations, such as a shift in side-chain rotamers, strength in ionic interactions, or relative positions of loops, may take place. Thus, pFXN protein is able to shift between thermodynamically different native-like states: in the extremes, an unstable (pH 8.0) and a stable one (pH 6.0), with an apparent p*Ka* = 7.34 (Fig. 3A). The narrow range of pH at which this high degree of stability modulation is observed leads us to think that histidine side-chains might be playing an important role, given that the p*Ka* of this residue is usually between 5 and 8 in proteins [57]. Although FXN structures from yeast, human, *E. coli*, and *P. ingrahamii* are almost superimposable, available thermodynamic data indicates that protein stability among homologs in the CyaY family can vary within a wide range. Illustrating this fact, unfolding free energy values are 5.6–7 [58] and 1.4 kcal mol^{-1} [49] for hFXN and yFXN variants, respectively. In addition, T_m values are 40.4 [49], 66.3–70 °C [58], for yFXN, hFXN, respectively, while pFXN T_m values vary from 35 to 53 °C (pH 8.0 and pH 6.0, respectively).

Regarding protein flexibility, a closer look at the protein structure shows that His44 and His67 residues, which are not conserved in the *E. coli* variant, are located in suggestive positions. As His44, Glu42, and Asp27 (the latter a residue of the acidic ridge) might establish an electrostatic network, and His67 is forming an ion pair with the buried Asp78 (5% of solvent exposed surface) we further investigated protein motions.

Analysis of MDS shows that the protonation state of His67 highly influences mobility of residues spanning positions 70–80. Further experiments are needed to determine whether these residues are modulators of protein flexibility and function in pFXN. Looking at the protein structure, one could reason that the protonation state of His67 might modulate the strength of interaction with Asp78, and thus, this interaction might tune the mobility in a pH dependent manner.

His44 interacts with Glu42 in the crystal structure. At a first glance, these residues do not seem to be participating in major tertiary interactions. However, His44 is structurally close to α1, β1 and loop1 (distance between γ carbons of Glu42 and Glu40 is 4.6 Å in the X-ray structure). The latter has been shown to be correlated to CTR fluctuations [51]. In addition, for the mesophilic variant eFXN, the NMR ensemble shows that the region concerning this loop and the CTR are highly correlated in their mobility (PDB ID: 1SOY). Moreover, truncation of this region leads to a protein that is highly sensitive in the region of loop 1 [51]. Thus, His44 might be involved in protein motions relevant for function. Our simulation results show that when Asp27 and Glu99 are close to each other (probably mediated by water interactions), residues Glu42 and His44 are close to each other as well.

Contrarily, when Asp27 is far from Glu99, the former interacts with Glu42, which is also far from His44. Moreover, Asp27 is included in the already mentioned acidic ridge involved in metal binding. Therefore, it is likely that metal ions might play a role in protein flexibility, by altering the electrostatic network.

The analysis of the RMSF calculated from our simulations shows that the highest values are found for residues 95 to 99 and 20 to 30 when neutral histidine tautomers are used. However, protonation of His44 or His67 decreases the mobility of these regions. Altogether, these results reinforce the idea of an interconnected electrostatic network that might be playing important roles in stability and mobility modulation, and perhaps, in pFXN function. Remarkably, the CTR of

Please cite this article as: E.A. Roman, et al., Frataxin from *Psychromonas ingrahamii* as a model to study stability modulation within the CyaY protein family, Biochim. Biophys. Acta (2012), http://dx.doi.org/10.1016/j.bbapap.2013.02.015

pFXN, which contains a cluster of negatively charged residues, displays significantly higher B-factor values in the case of pFXN than in *E. coli* homolog. As FXN iron binding sites occur within clusters of Glu/Asp residues, we propose that the CTR might alter the biological function dynamics through flexibility and stability modulations based on ligand binding. This is reinforced by MDS results which point to a correlation between motions of residues in the CTR, and residues of α1, β1 and loop1.

5. Conclusion

In our work, we give structural information about *P. ingrahamii* frataxin variant stability. We found that it is highly modulated by pH, in contrast with other variants previously reported. The analysis of the pFXN structure suggests that an electrostatic network of interactions might participate in the modulation of global stability and local mobility. In silico results showed that histidine residues are located in highly mobile regions of the protein. Moreover, we have shown that pFXN flexibility may be significantly altered by the modulation of the protonation state at specific sites. Further NMR analysis accompanied by simplified simulations at different pH values, taking into account electrostatic contribution, may aid in the analysis of the relations between flexibility and stability.

Acknowledgements

This work was supported by Agencia Nacional de Promoción Científica y Tecnológica (ANPCyT), Consejo Nacional de Investigaciones Científicas y Técnicas (CONICET) and Universidad de Buenos Aires (UBACyT). We also acknowledge Dr. Patricio O. Craig, Esteban Lanzarotti, and Dr. Mariano C. Gonzalez Lebrero for valuable comments on data analysis. We specially thank the IGBMC Structural Genomics platform staff (in particular, Pierre Poussin Courmontagne and Dr. Alastair McEwen). Crystallographic experiments were performed on the X06DA beamline at the Swiss Light Source, Paul Scherrer Institut, Villigen, Switzerland. In particular, we thank Christian Stirnimann, Vincent Olieric and Meitian Wan for their help on the beamline.

Appendix A. Supplementary data

Supplementary data to this article can be found online at http://dx.doi.org/10.1016/j.bbapap.2013.02.015.

References

[1] M. Desjardins, L.A. Graham, P.L. Davies, G.L. Fletcher, Antifreeze protein gene amplification facilitated niche exploitation and speciation in wolffish, FEBS J. 279 (2012) 2215–2230.
[2] G.L. Fletcher, C.L. Hew, P.L. Davies, Antifreeze proteins of teleost fishes, Annu. Rev. Physiol. 63 (2001) 359–390.
[3] M. Hebraud, P. Potier, Cold shock response and low temperature adaptation in psychrotrophic bacteria, J. Mol. Microbiol. Biotechnol. 1 (1999) 211–219.
[4] S. D'Amico, T. Collins, J.C. Marx, G. Feller, C. Gerday, Psychrophilic microorganisms: challenges for life, EMBO Rep. 7 (2006) 385–389.
[5] W.R. Driedzic, K.V. Ewart, Control of glycerol production by rainbow smelt (*Osmerus mordax*) to provide freeze resistance and allow foraging at low winter temperatures, Comp. Biochem. Physiol. B Biochem. Mol. Biol. 139 (2004) 347–357.
[6] G. Feller, Protein stability and enzyme activity at extreme biological temperatures, J. Phys. Condens. Matter 22 (2010) 323101.
[7] F. Piette, C. Struvay, G. Feller, The protein folding challenge in psychrophiles: facts and current issues, Environ. Microbiol. 13 (2011) 1924–1933.
[8] A. Cipolla, F. Delbrassine, J.L. Da Lage, G. Feller, Temperature adaptations in psychrophilic, mesophilic and thermophilic chloride-dependent alpha-amylases, Biochimie 94 (2012) 1943–1950.
[9] S. Davail, G. Feller, E. Narinx, C. Gerday, Cold adaptation of proteins. Purification, characterization, and sequence of the heat-labile subtilisin from the antarctic psychrophile *Bacillus* TA41, J. Biol. Chem. 269 (1994) 17448–17453.
[10] E. Papaleo, M. Tiberti, G. Invernizzi, M. Pasi, V. Ranzani, Molecular determinants of enzyme cold adaptation: comparative structural and computational studies of cold- and warm-adapted enzymes, Curr. Protein Pept. Sci. 12 (2011) 657–683.
[11] K.S. Siddiqui, R. Cavicchioli, Cold-adapted enzymes, Annu. Rev. Biochem. 75 (2006) 403–433.
[12] A.O. Smalas, H.K. Leiros, V. Os, N.P. Willassen, Cold adapted enzymes, Biotechnol. Annu. Rev. 6 (2000) 1–57.
[13] R. Chiuri, G. Maiorano, A. Rizzello, L.L. del Mercato, R. Cingolani, R. Rinaldi, M. Maffia, P.P. Pompa, Exploring local flexibility/rigidity in psychrophilic and mesophilic carbonic anhydrases, Biophys. J. 96 (2009) 1586–1596.
[14] N.G. Assefa, L. Niiranen, N.P. Willassen, A. Smalas, E. Moe, Thermal unfolding studies of cold adapted uracil-DNA N-glycosylase (UNG) from Atlantic cod (*Gadus morhua*). A comparative study with human UNG, Comp. Biochem. Physiol. B Biochem. Mol. Biol. 161 (2012) 60–68.
[15] C. Struvay, G. Feller, Optimization to low temperature activity in psychrophilic enzymes, Int. J. Mol. Sci. 13 (2012) 11643–11665.
[16] P. Falasca, G. Evangelista, R. Cotugno, S. Marco, M. Masullo, E. De Vendittis, G. Raimo, Properties of the endogenous components of the thioredoxin system in the psychrophilic eubacterium *Pseudoalteromonas haloplanktis* TAC 125, Extremophiles 16 (2012) 539–552.
[17] A. Miranda-Vizuete, A.E. Damdimopoulos, J. Gustafsson, G. Spyrou, Cloning, expression, and characterization of a novel *Escherichia coli* thioredoxin, J. Biol. Chem. 272 (1997) 30841–30847.
[18] P. Mereghetti, L. Riccardi, B.O. Brandsdal, P. Fantucci, L. De Gioia, E. Papaleo, Near native-state conformational landscape of psychrophilic and mesophilic enzymes: probing the folding funnel model, J. Phys. Chem. B 114 (2010) 7609–7619.
[19] G. Musco, G. Stier, B. Kolmerer, S. Adinolfi, S. Martin, T. Frenkiel, T. Gibson, A. Pastore, Towards a structural understanding of Friedreich's ataxia: the solution structure of frataxin, Structure 8 (2000) 695–707.
[20] M. Pandolfo, A. Pastore, The pathogenesis of Friedreich ataxia and the structure and function of frataxin, J. Neurol. 256 (Suppl. 1) (2009) 9–17.
[21] C.C. Philpott, Coming into view: eukaryotic iron chaperones and intracellular iron delivery, J. Biol. Chem. 287 (2012) 13518–13523.
[22] J. Bridwell-Rabb, C. Iannuzzi, A. Pastore, D.P. Barondeau, Effector role reversal during evolution: the case of frataxin in Fe–S cluster biosynthesis, Biochemistry 51 (2012) 2506–2514.
[23] Y. He, S.L. Alam, S.V. Proteasa, Y. Zhang, E. Lesuisse, A. Dancis, T.L. Stemmler, Yeast frataxin solution structure, iron binding, and ferrochelatase interaction, Biochemistry 43 (2004) 16254–16262.
[24] M. Nair, S. Adinolfi, C. Pastore, G. Kelly, P. Temussi, A. Pastore, Solution structure of the bacterial frataxin ortholog, CyaY: mapping the iron binding sites, Structure 12 (2004) 2037–2048.
[25] S. Adinolfi, M. Nair, A. Politou, E. Bayer, S. Martin, P. Temussi, A. Pastore, The factors governing the thermal stability of frataxin orthologues: how to increase a protein's stability, Biochemistry 43 (2004) 6511–6518.
[26] M. Riley, J.T. Staley, A. Danchin, T.Z. Wang, T.S. Brettin, L.J. Hauser, M.L. Land, L.S. Thompson, Genomics of an extreme psychrophile, *Psychromonas ingrahamii*, BMC Genomics 9 (2008) 210.
[27] A.J. Auman, J.L. Breezee, J.J. Gosink, P. Kampfer, J.T. Staley, *Psychromonas ingrahamii* sp. nov., a novel gas vacuolate, psychrophilic bacterium isolated from Arctic polar sea ice, Int. J. Syst. Evol. Microbiol. 56 (2006) 1001–1007.
[28] A.J. Auman, J.L. Breezee, J.J. Gosink, P. Schumann, C.R. Barnes, P. Kampfer, J.T. Staley, *Psychromonas boydii* sp. nov., a gas-vacuolate, psychrophilic bacterium isolated from an Arctic sea-ice core, Int. J. Syst. Evol. Microbiol. 60 (2010) 84–92.
[29] J. Breezee, N. Cady, J.T. Staley, Subfreezing growth of the sea ice bacterium "*Psychromonas ingrahamii*", Microb. Ecol. 47 (2004) 300–304.
[30] J. Navaza, Implementation of molecular replacement in AMoRe, Acta Crystallogr. D: Biol. Crystallogr. 57 (2001) 1367–1372.
[31] S. Trapani, J. Navaza, AMoRe: classical and modern, Acta Crystallogr. D: Biol. Crystallogr. 64 (2008) 11–16.
[32] J. Navaza, AMoRe: an automated package for molecular replacement, Acta Crystallogr. Sect. A 50 (1994) 157–163.
[33] P. Emsley, B. Lohkamp, W.G. Scott, K. Cowtan, Features and development of Coot, Acta Crystallogr. D: Biol. Crystallogr. 66 (2010) 486–501.
[34] P.D. Adams, P.V. Afonine, G. Bunkoczi, V.B. Chen, I.W. Davis, N. Echols, J.J. Headd, L.W. Hung, G.J. Kapral, R.W. Grosse-Kunstleve, A.J. McCoy, N.W. Moriarty, R. Oeffner, R.J. Read, D.C. Richardson, J.S. Richardson, T.C. Terwilliger, P.H. Zwart, PHENIX: a comprehensive Python-based system for macromolecular structure solution, Acta Crystallogr. D: Biol. Crystallogr. 66 (2010) 213–221.
[35] M.M. Santoro, D.W. Bolen, Unfolding free energy changes determined by the linear extrapolation method. 1. Unfolding of phenylmethanesulfonyl alpha-chymotrypsin using different denaturants, Biochemistry 27 (1988) 8063–8068.
[36] M.M. Santoro, D.W. Bolen, A test of the linear extrapolation of unfolding free energy changes over an extended denaturant concentration range, Biochemistry 31 (1992) 4901–4907.
[37] C. Oostenbrink, A. Villa, A.E. Mark, W.F. van Gunsteren, A biomolecular force field based on the free enthalpy of hydration and solvation: the GROMOS force-field parameter sets 53A5 and 53A6, J. Comput. Chem. 25 (2004) 1656–1676.
[38] H.J.C. Berendsen, J.R. Grigera, T.P. Straatsma, The missing term in effective pair potentials, J. Chem. Phys. 91 (2002) 6269–6271.
[39] H.J.C. Berendsen, J.P.M. Postma, W.F.v. Gunsteren, A. DiNola, J.R. Haak, Molecular dynamics with coupling to an external bath, J. Chem. Phys. 81 (1984) 3684–3690.
[40] K.G. Tina, R. Bhadra, N. Srinivasan, PIC: protein interactions calculator, Nucleic Acids Res. 35 (2007) W473–W476.
[41] Y. Chen, M.D. Barkley, Toward understanding tryptophan fluorescence in proteins, Biochemistry 37 (1998) 9976–9982.
[42] D. Peak, Fluorescence quenching at high quencher concentrations, J. Chem. Phys. 79 (1983) 3328–3335.

Please cite this article as: E.A. Roman, et al., Frataxin from *Psychromonas ingrahamii* as a model to study stability modulation within the CyaY protein family, Biochim. Biophys. Acta (2012), http://dx.doi.org/10.1016/j.bbapap.2013.02.015

[43] A.C. King, M. Woods, W. Liu, Z. Lu, D. Gill, M.R. Krebs, High-throughput measurement, correlation analysis, and machine-learning predictions for pH and thermal stabilities of Pfizer-generated antibodies, Protein Sci. 20 (2011) 1546–1557.
[44] C.J. Layton, H.W. Hellinga, Thermodynamic analysis of ligand-induced changes in protein thermal unfolding applied to high-throughput determination of ligand affinities with extrinsic fluorescent dyes, Biochemistry 49 (2010) 10831–10841.
[45] C.J. Layton, H.W. Hellinga, Quantitation of protein–protein interactions by thermal stability shift analysis, Protein Sci. (2011) 1439–1450.
[46] J. Vertrees, P. Barritt, S. Whitten, V.J. Hilser, COREX/BEST server: a web browser-based program that calculates regional stability variations within protein structures, Bioinformatics 21 (2005) 3318–3319.
[47] J.O. Wrabl, V.J. Hilser, Investigating homology between proteins using energetic profiles, PLoS Comput. Biol. 6 (2010) e1000722.
[48] J. Schymkowitz, J. Borg, F. Stricher, R. Nys, F. Rousseau, L. Serrano, The FoldX web server: an online force field, Nucleic Acids Res. 33 (2005) W382–W388.
[49] A.R. Correia, T. Wang, E.A. Craig, C.M. Gomes, Iron-binding activity in yeast frataxin entails a trade off with stability in the alpha1/beta1 acidic ridge region, Biochem. J. 426 (2010) 197–203.
[50] I. Walsh, G. Minervini, A. Corazza, G. Esposito, S.C. Tosatto, F. Fogolari, Bluues server: electrostatic properties of wild-type and mutated protein structures, Bioinformatics 28 (2012) 2189–2190.
[51] E.A. Roman, S.E. Faraj, M. Gallo, A.G. Salvay, D.U. Ferreiro, J. Santos, Protein stability and dynamics modulation: the case of human frataxin, PLoS One 7 (2012) e45743.
[52] A.L. Bulteau, H.A. O'Neill, M.C. Kennedy, M. Ikeda-Saito, G. Isaya, L.I. Szweda, Frataxin acts as an iron chaperone protein to modulate mitochondrial aconitase activity, Science 305 (2004) 242–245.
[53] M.V. Maliandi, M.V. Busi, V.R. Turowski, L. Leaden, A. Araya, D.F. Gomez-Casati, The mitochondrial protein frataxin is essential for heme biosynthesis in plants, FEBS J. 278 (2011) 470–481.
[54] E. Napoli, F. Taroni, G.A. Cortopassi, Frataxin, iron–sulfur clusters, heme, ROS, and aging, Antioxid. Redox Signal. 8 (2006) 506–516.
[55] T.L. Stemmler, E. Lesuisse, D. Pain, A. Dancis, Frataxin and mitochondrial FeS cluster biogenesis, J. Biol. Chem. 285 (2010) 26737–26743.
[56] R.A. Vaubel, G. Isaya, Iron–sulfur cluster synthesis, iron homeostasis and oxidative stress in Friedreich ataxia, Mol. Cell. Neurosci. (2012). Q10
[57] A. Fersht, Structure and Mechanism in Protein Science: A Guide to Enzyme Catalysis and Protein Folding, W. H. Freeman, 1998.
[58] A.R. Correia, C. Pastore, S. Adinolfi, A. Pastore, C.M. Gomes, Dynamics, stability and iron-binding activity of frataxin clinical mutants, FEBS J. 275 (2008) 3680–3690.
[59] J.K. Myers, C.N. Pace, J.M. Scholtz, Denaturant m values and heat capacity changes: relation to changes in accessible surface areas of protein unfolding, Protein Sci. 4 (1995) 2138–2148.

Please cite this article as: E.A. Roman, et al., Frataxin from *Psychromonas ingrahamii* as a model to study stability modulation within the CyaY protein family, Biochim. Biophys. Acta (2012), http://dx.doi.org/10.1016/j.bbapap.2013.02.015